Controlled Approach Strategies on Small Celestial Bodies Using Approximate Analytical Solutions of the Elliptical Three-Body Problem: Application to the Mars-Phobos System

Rui M. S. Martins*
Instituto Superior Técnico, 1049-001 Lisbon, Portugal

***Abstract*—In this thesis, quasi-satellite orbits in the elliptic restricted three-body problem are studied from a preliminary mission design point of view. A description of such orbits and their long-term evolution is given, and the stability conditions investigated are used for the case of the Mars-Phobos system. A first-order solution on the osculating elements is obtained with the use of perturbation theories and validation is performed using the numerical model as comparison term. A trajectory design algorithm is developed using the obtained analytical solutions with the purpose of studying different approach strategies to the Martian moon. An energy consumption analysis is performed to understand which strategy is more efficient in terms of fuel consumption. Due to the approximations made, the obtained analytical solutions have low validity when in close proximity to Phobos, as a result a control procedure is introduced onto the trajectory algorithm, which performs timely corrections to the actual trajectory. Two landing scenarios are considered providing some flexibility in terms of mission design.**

***Keywords*—Quasi-Satellite Orbits, Elliptic Restricted Three-Body Problem, Variation of Parameters, Differential Evolution, Mars-Phobos System.**

I. Introduction

SMALL bodies of the solar system, such as Phobos, cannot be circumnavigated in Keplerian-type orbits because, in the context of the three-body problem (3BP), the Lagrange points are very close to the surface of the small body and the region of influence of the small body ends below its surface [1]. This makes the problem of orbiting small bodies more difficult to solve because it is necessary to account for the gravitational attraction of the larger body of the system, which in our case is Mars.

The special interest for Phobos results from the fact that the Martian moon is one of the most prominent destinations for future scientific missions, and discovering its unknown origin and understanding its basic scientific nature could provide some insight about the evolution of planets and small bodies of our solar system [2]. Also, the parameters of the problem make it particularly difficult to solve [1]. The eccentricity of Phobos' orbit and its gravitational parameter μ_{Ph} are relatively high with respect to other small bodies of the solar system. Therefore, by solving the problem for Phobos' case and testing its validity will enable the use of these solutions for other interesting bodies of the solar system, which have smaller μ and orbital eccentricity.

To land on Phobos it is crucial to first determine an adequate landing site, which requires orbiting the moon and performing observations from a distance. Although it is not possible to orbit the moon in a Keplerian way, it is still possible to do it using a special kind of orbits called QSO's [1]. Such orbits exist beyond the Lagrange points, as seen from the synodic reference frame usually used in the three-body problem. The reference frame's origin is located at the centre of Phobos and rotates with the angular velocity of Phobos around Mars.

The trajectory that the S/C performs around Phobos does not fit well the concept of orbit in the usual sense of a perturbed Keplerian trajectory so, for convenience of description, the term epicycle will be used to designate each orbit of the S/C around Phobos in the synodic reference frame while the term QSO will be used to describe the entire dynamics of the epicycles.

In this configuration, it is possible to describe a coplanar QSO relative to the orbital plane of Phobos as a retrograde motion in elliptical epicycles that drift forward and backwards in the direction of the orbital velocity of the moon. In Fig. 1 it is presented the difference between two S/C orbits around Phobos when we take into account Phobos' gravity and when the gravity of Phobos is neglected. As it is possible to observe in Fig. 1, the motion of a S/C in the vicinity of Phobos is considerably different when we account for its gravity. This shows that Phobos' gravity must be taken into account; in general it tends to stabilize the motion of the S/C around it, but depending on the initial conditions it may have the opposite effect [1]. Theoretically when the motion is stable, the epicycles continue to drift back and forth indefinitely. In practice, the perturbation forces cause the S/C to eventually drift away, which means that stability can only be assured for a sufficiently long period of time.

*M. Sc. Candidate, Department of Mechanical Engineering, Avenue Rovisco Pais, Instituto Superior Técnico; rui.s.martins@ist.utl.pt

The present work was performed under the supervision of Paulo J. S. Gil, Assistant Professor, Department of Mechanical Engineering, Instituto Superior Técnico, UTL, Avenue Rovisco Pais.

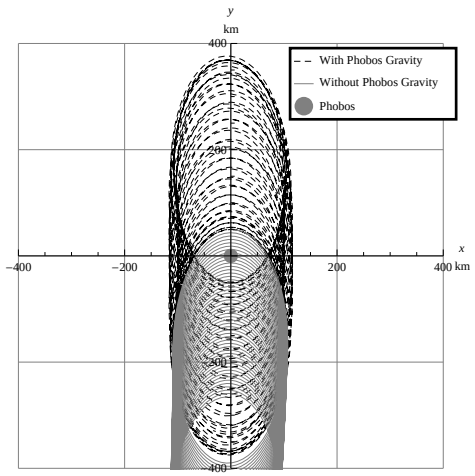

Fig. 1: Difference between two S/C orbits around Phobos when we take into a account Phobos' gravity and when the gravity of Phobos is neglected. Initial conditions: $(x, y, z) = (0, 50, 0)$ $[km]$ and $(v_x, v_y, v_z) = (25, 0, 0)$ $[m/s]$.

II. Analytical Solutions

The equations of motion for the three dimensional elliptic restricted three body problem in pulsating variables are [3]:

$$\begin{aligned}
\frac{d^2x}{df^2} &= 2\frac{dy}{df} + \frac{1}{1+e\cos f}\left(3x - \frac{x}{R_2^3}\right),\\
\frac{d^2y}{df^2} &= -2\frac{dx}{df} - \frac{1}{1+e\cos f}\left(\frac{y}{R_2^3}\right),\\
\frac{d^2z}{df^2} &= -z - \frac{1}{1+e\cos f}\left(\frac{z}{R_2^3}\right),
\end{aligned} \tag{1}$$

where e and f represent the eccentricity and the true anomaly of the orbit of Phobos, while R_1 and R_2 are the distance of the third body to Mars and Phobos, respectively.

A. Force Free Hill's Equations

When the orbit becomes large enough the term $R_2^{-3} \to 0$ allowing us to neglect, as a first approximation, the last term of each equation on the right-hand side of (1) leading to [4], [5]:

$$\begin{aligned}
\frac{d^2x}{df^2} &= 2\frac{dy}{df} + \frac{3x}{1+e\cos f},\\
\frac{d^2y}{df^2} &= -2\frac{dx}{df},\\
\frac{d^2z}{df^2} &= -z.
\end{aligned} \tag{2}$$

The resultant equations represent a set of ordinary differential equations with time-dependent periodic coefficients. There is no explicit method of finding the solution of this type of systems. However, it is possible to find the solution in x and y using the program *Wolfram Mathematica*® to obtain one independent solution and then use the method described in [6], [7] to obtain the second independent solution from the first.

The resulting solutions for x and y are too complicated to draw any conclusions about the motion of a S/C in the vicinity of Phobos. So given the fact that the eccentricity of the orbit of Phobos is small ($e = 0.0151$), it is possible to simplify the obtained solutions using a series expansion with respect to the eccentricity, centered around $e = 0$, omitting the terms of the second and higher orders, resulting in

$$\begin{aligned}
x(f) =& (1 + e\cos f)(C_1 \sin f + C_2 \cos f)\\
&-2eC_2 + 2C_3 - eC_3 \cos f - 3eC_3 f \sin f,\\
y(f) =& (2 + e\cos f)(C_1 \cos f - C_2 \sin f)\\
&-\frac{1}{2}eC_1 + 3eC_2 f - 3C_3 f + 8eC_3 \sin f\\
&-6eC_3 f \cos f + C_4,\\
z(f) =& Z_1 \cos f + Z_2 \sin f,
\end{aligned} \tag{3}$$

where C_i and Z_i are integration constants that can be derived from the initial conditions of the problem. Equation (3) represent the analytical solution for the force free Hill's equations of the Three-Dimensional Elliptic Restricted Three Body Problem (ER3BP).

Figure 2 illustrates an example of the solutions resultant from the expressions in Eq. (3).

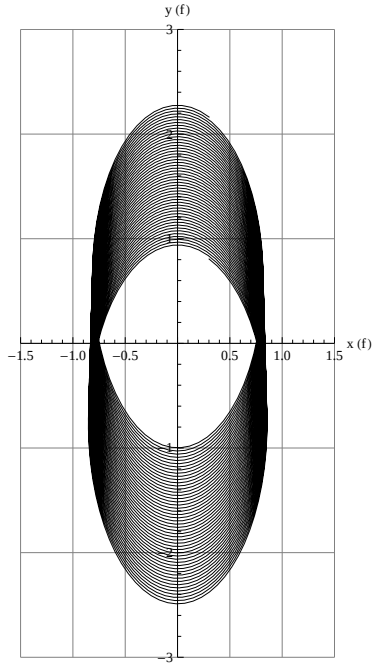

Fig. 2: Parametric plot of the approximate analytical solutions of the unperturbed equations for $e = 0.0151$, $C_1 = 0.8$, $C_2 = 0.3$, $C_3 = 0.03$ and $C_4 = -0.8$.

B. Osculating parameters

The physically meaningful quantities in (3) are, rather than the C_i and Z_i parameters, the semi-minor axis A of the epicycle, the coordinates δ_x and δ_y of the centre of the epicycle, the phase difference ϕ between the motion of the S/C around Phobos and the motion of Phobos around Mars, the parameter γ for the amplitude of the harmonic oscillations with respect to the plane $z = 0$, and the parameter ψ as the phase of the oscillations along the z direction. The last parameter β describes the inclination relative to the x-axis of the line of intersection between the plane of the epicycle and the $x - y$ plane. These parameters are graphically represented in Fig. 3 and can be defined as:

$$
\begin{aligned}
A =& (C_1^2 + C_2^2)^{\frac{1}{2}} \\
\phi =& \arctan\left(-\frac{C_1}{C_2}\right) \\
\delta_x =& -2eC_2 + 2C_3 - eC_3\cos f - 3eC_3 f \sin f \\
\delta_y =& -\frac{1}{2}eC_1 + 3eC_2 f - 3C_3 f + 8eC_3 \sin f \\
& - 6eC_3 f \cos f + C_4 \\
\gamma =& (Z_1^2 + Z_2^2)^{\frac{1}{2}} \\
\psi =& \arctan\left(-\frac{Z_2}{Z_1}\right) \\
\beta =& \psi - \phi.
\end{aligned}
\tag{4}
$$

The parameters in (4) are called osculating parameters because they describe an osculating orbit, which is the orbit that a S/C would assume if at some instant in time the S/C was not subject to perturbations. However, real orbits experience perturbations which may cause the osculating elements to evolve in time. As a result we consider the motion of the S/C as a continuous transition from one osculating orbit to another osculating orbit.

Using (4) in Eqs.(3) it is possible to rewrite the solutions of the force free Hill's equations as:

$$
\begin{aligned}
x(f) &= (1 + e\cos f)A\cos(f + \phi) + \delta_x, \\
y(f) &= -(2 + e\cos f)A\sin(f + \phi) + \delta_y, \\
z(f) &= \gamma\cos(f + \psi).
\end{aligned}
\tag{5}
$$

According to (4), we can assume that the terms A, ϕ, γ and ψ are constants and that only δ_x and δ_y are time-dependent. Differentiating the expressions of δ_x and δ_y in (4) leads to:

$$
\begin{aligned}
\dot{\delta}_x &= -2eC_3\sin f - 3eC_3 f\cos f \\
\dot{\delta}_y &= -3C_3 + 3eA\cos\phi + 2eC_3\cos f + 6eC_3 f\sin f.
\end{aligned}
\tag{6}
$$

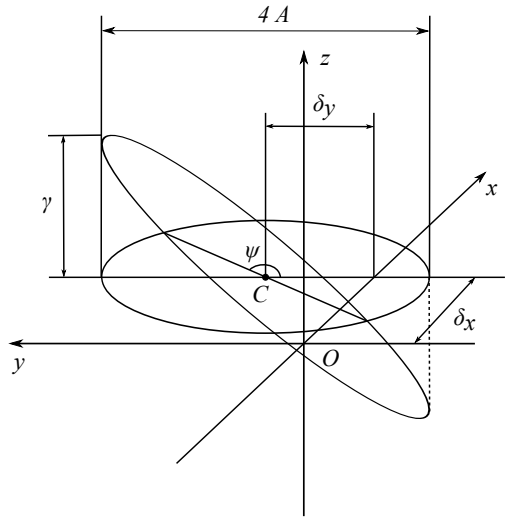

Fig. 3: Geometric representation of the osculating parameters. O is the origin of the Cartesian reference frame and C is the epicycles center. Figure adapted from [1].

It is possible to observe from (6) that the derivatives of δ_x and δ_y are linearly dependent of the term $eC_3 f$. As a result, if the term $C_3 \neq 0$, the variation of both parameters will increase over time, which in turn will lead to orbital instability. To select stable solutions we must set $C_3 = 0$, ensuring that the position of the center of the epicycle does not present secular variation. Thus, the expressions for δ_x, δ_y and its respective derivatives can be rewritten as:

$$
\begin{aligned}
\delta_x &= -2eA\cos\phi, \\
\delta_y &= \tfrac{1}{2}eA\sin\phi + 3efA\cos\phi + C_4, \\
\dot{\delta}_x &= 0, \\
\dot{\delta}_y &= 3eA\cos\phi.
\end{aligned}
\tag{7}
$$

C. Variation of Parameters

The osculating elements were introduced in order to better describe the motion of a S/C orbiting Phobos. However, only the case of sufficiently large orbits was considered. For such configuration it was assumed that the osculating parameters would be constant except for δ_y.

Now, in order to account for the last term of each equation on the right-hand side of (1), it will be assumed that these osculating elements may vary in time. To obtain the approximate solutions of the ER3BP we use the method of variation of parameters to derive the differential equations that define the variation of the osculating elements [8]. However the result is too complex to conclude about the system behaviour. So, for the case of interest, i.e. the Mars-Phobos system, we simplify the problem by assuming that $e \ll 1$, $\frac{\delta_x}{A} \ll 1$, $\frac{\delta_y}{A} \ll 1$ and $\frac{\gamma}{A} \ll 1$. Doing a series expansion of the approximate solutions

with respect to the mentioned quantities, centered around zero and considering only the first order terms, and averaging the result over the period of 2π will result in the following average equations for the osculating parameters:

$$\begin{aligned}
&\dot{\bar{A}} = 0,\\
&\dot{\bar{\phi}} = \tfrac{K}{\pi \bar{A}^3},\\
&\dot{\bar{\delta}}_x = \tfrac{2}{3\pi \bar{A}^3}(K-E)\ \bar{\delta}_y + \tfrac{2}{9\pi \bar{A}^2}(7E-K)\ e\ \sin\phi,\\
&\dot{\bar{\delta}}_y = \left(-\tfrac{3}{2} + \tfrac{2}{3\pi \bar{A}^3}(K-4E)\right)\ \bar{\delta}_x - \tfrac{2}{\pi \bar{A}^2}\ e\ \cos\phi,\\
&\dot{\bar{\gamma}} = \tfrac{1}{6\pi \bar{A}^3}(5E-2K)\gamma \sin\left(2\bar{\beta}\right),\\
&\dot{\bar{\psi}} = \tfrac{1}{6\pi \bar{A}^3}\left(3E + (5E-2K)\cos\left(2\bar{\beta}\right)\right),\\
&\dot{\bar{\beta}} = \tfrac{1}{6\pi \bar{A}^3}\left((3E-6K) + (5E-2K)\cos\left(2\bar{\beta}\right)\right),
\end{aligned} \tag{8}$$

where the constants K and E are complete elliptic integrals of modulus $k = \frac{\sqrt{3}}{2}$. It is interesting to know that when the eccentricity is set to zero ($e = 0$) this equations become identical to the ones of the zero eccentricity case [4], as expected.

D. Solutions of the Averaged Equations

After computing the average differential equations on the osculating parameters, it is possible to obtain a solution to describe the motion of a S/C orbiting Phobos. This is accomplished by integrating the system in (8). For the sake of simplicity the bar superscript was removed from the variables. The differential equations on A and ϕ are easily solvable and take the form

$$\begin{aligned}
&A = \text{constant}\\
&\phi = \tfrac{K}{\pi A^3}(f - f_0) + \phi_0,
\end{aligned} \tag{9}$$

where f_0 is the initial true anomaly of the Orbit of Phobos and ϕ_0 the initial phase difference between the motion of the S/C about Phobos and the motion Phobos about Mars, as depicted in Fig. 4.

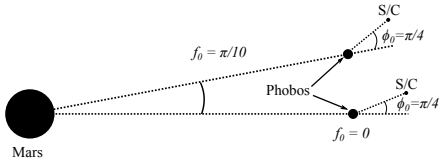

Fig. 4: Geometric representation of the parameters f_0 and ϕ_0 for two distinct cases. In the first one $f_0 = 0$ and $\phi_0 = \frac{\pi}{4}$ and in the second $f_0 = \frac{\pi}{10}$ and $\phi_0 = \frac{\pi}{4}$.

The remaining four equations can be separated into two subsystems, the first describing the drift oscillations (the variables $\bar{\delta}_x$ and $\bar{\delta}_y$) while the second relates the precession of the plane of the epicycle (the variables $\bar{\gamma}$ and $\bar{\psi}$). Integration of the first subsystem gives the solution

$$\begin{aligned}
\delta_x =& Q_1 \cos\left[\sqrt{P_2 P_4} f\right] + Q_2 \sqrt{\frac{P_2}{P_4}} \sin\left[\sqrt{P_2 P_4} f\right]\\
&- \frac{P_1 P_3 + P_2 P_5}{P_1^2 - P_2 P_4} e \cos\left[P_1 (f - f_0) + \phi_0\right]\\
\delta_y =& Q_2 \cos\left[\sqrt{P_2 P_4} f\right] - Q_1 \sqrt{\frac{P_4}{P_2}} \sin\left[\sqrt{P_2 P_4} f\right]\\
&+ \frac{P_3 P_4 + P_1 P_5}{P_1^2 - P_2 P_4} e \sin\left[P_1 (f - f_0) + \phi_0\right],
\end{aligned} \tag{10}$$

where the constants (P_1, P_2, P_3, P_4, P_5, Q_1, Q_2) are defined as:

$$\begin{aligned}
P_1 =& \frac{K}{\pi A^3}, \qquad P_2 = \frac{2}{3\pi A^3}(K - E),\\
P_3 =& \frac{2}{9\pi A^2}(7E - K),\\
P_4 =& \frac{3}{2} - \frac{2}{3\pi A^3}(K - 4E), \qquad P_5 = \frac{2}{\pi A^2},
\end{aligned}$$

$$\begin{aligned}
Q_1 =& \delta_{x0} \cos\left[\sqrt{P_2 P_4} f_0\right] + \sqrt{\frac{P_2}{P_4}} \delta_{y0} \sin\left[\sqrt{P_2 P_4} f_0\right]\\
&+ e \left(\frac{P_1 P_3 + P_2 P_5}{P_1^2 - P_2 P_4} \cos\left[\sqrt{P_2 P_4} f_0\right] \cos\phi_0 \right.\\
&\left. + \sqrt{\frac{P_2}{P_4}}\ \frac{P_3 P_4 + P_1 P_5}{P_1^2 + P_2 P_4} \sin\left[\sqrt{P_2 P_4} f_0\right] \sin\phi_0 \right),
\end{aligned} \tag{11}$$

$$\begin{aligned}
Q_2 =& \sqrt{\frac{P_4}{P_2}} \delta_{x0} \sin\left[\sqrt{P_2 P_4} f_0\right] + \delta_{y0} \cos\left[\sqrt{P_2 P_4} f_0\right]\\
&+ e \left(\sqrt{\frac{P_4}{P_2}}\ \frac{P_1 P_3 + P_2 P_5}{P_1^2 - P_2 P_4} \sin\left[\sqrt{P_2 P_4} f_0\right] \cos\phi_0 \right.\\
&\left. - \frac{P_3 P_4 + P_1 P_5}{P_1^2 - P_2 P_4} \cos\left[\sqrt{P_2 P_4} f_0\right] \sin\phi_0 \right).
\end{aligned}$$

The second subsystem is independent on the variable β and its solution is

$$\beta = \arctan\left[\sqrt{\frac{P_6^2 + P_7^2}{P_6^2 - P_7^2}} \tan\left(\sqrt{P_6^2 - P_7^2} \left[(f - f_0) + \beta_0\right] \right) \right], \tag{12}$$

where β_0 is a constant and P_6 and P_7 are:

$$P_6 = \tfrac{3E-6K}{6\pi \bar{A}^3}, \qquad P_7 = \tfrac{5E-2K}{6\pi \bar{A}^3}. \tag{13}$$

It is clear from (12) that the intersection of the plane of the epicycle and the $z = 0$ plane rotates in the direction of the motion along the epicycle with an average velocity

$$\omega_\beta = \frac{2}{3\pi A^3} \sqrt{2K^2 - EK - E^2} \approx 0.484965 A^{-3}. \tag{14}$$

After the substitution of β the solution on γ is obtained

$$\gamma = \frac{\gamma_0}{\sqrt{P_6 + P_7 \cos 2\beta}}, \tag{15}$$

indicating that the amplitude of the z-oscillations vary periodically with frequency $2\omega_\beta$. Finally, using (9) - (15) and applying them in (5) we can write the approximate solutions of the ER3BP in osculating parameters:

$$\begin{aligned} x &= (1 + e\cos[f - f_0])A\cos[(1+P_1)(f-f_0)+\phi_0] \\ &+ Q_1 \cos\left[\sqrt{P_2P_4}f\right] + Q_2\sqrt{\frac{P_2}{P_4}}\sin\left[\sqrt{P_2P_4}f\right] \\ &- \frac{P_1P_3 + P_2P_5}{P_1^2 - P_2P_4} e\cos[P_1(f-f_0)+\phi_0], \\ y &= -(2 + e\cos[f - f_0])A\sin[(1+P_1)(f-f_0)+\phi_0] \\ &+ Q_2 \cos\left[\sqrt{P_2P_4}f\right] - Q_1\sqrt{\frac{P_4}{P_2}}\sin\left[\sqrt{P_2P_4}f\right] \\ &+ \frac{P_3P_4 + P_1P_5}{P_1^2 - P_2P_4} e\sin[P_1(f-f_0)+\phi_0], \end{aligned} \tag{16}$$

$$z = \frac{\gamma_0 \cos\left((1+P_1)(f-f_0)+\phi_0 + \arctan\left[\sqrt{\frac{P_6^2+P_7^2}{P_6^2-P_7^2}}\tan\left(\sqrt{P_6^2-P_7^2}\,[(f-f_0)+\beta_0]\right)\right]\right)}{\sqrt{P_6 + P_7\cos\left(2\arctan\left[\sqrt{\frac{P_6^2+P_7^2}{P_6^2-P_7^2}}\tan\left(\sqrt{P_6^2-P_7^2}\,[(f-f_0)+\beta_0]\right)\right]\right)}}$$

E. Period Analysis

With the obtained solutions (16) it is possible to identify 4 main periodic motions within the dynamics around Phobos. The revolution about the epicycle is one of the periodic motions and has a similar period to the period of the orbit of Phobos about Mars (that is why the orbits are denominated quasi-synchronous). Its value is

$$\tau_1 = \frac{2\pi}{1+P_1} = \frac{2\pi}{1 + \frac{K}{\pi A^3}}, \tag{17}$$

(the period of Phobos' orbit is 2π in the dimensionless units used). For smaller amplitudes (A) the difference to Phobos orbital period increases since the terms $\frac{x}{R}$, $\frac{y}{R}$, $\frac{z}{R}$ are no longer small, which explains this approximation solutions low validity. The oscillations of the epicycle's center are composed by two distinct periodic motions. The first one has a period of

$$\tau_2 = \frac{2\pi}{\sqrt{P_2P_4}} \approx \frac{14.0275A^3}{\sqrt{0.570359 + \frac{3}{2}A^3}}, \tag{18}$$

and its amplitude is composed by terms that depend on the eccentricity of the orbit of Phobos and terms that depend on the initial position of the center of the epicycle (δ_{x0} and δ_{y0}), while the second periodic motion has a period of

$$\tau_3 = \frac{2\pi}{\dot{\phi}} = \frac{2\pi}{\frac{K}{\pi A^3}} \approx 9.15328A^3. \tag{19}$$

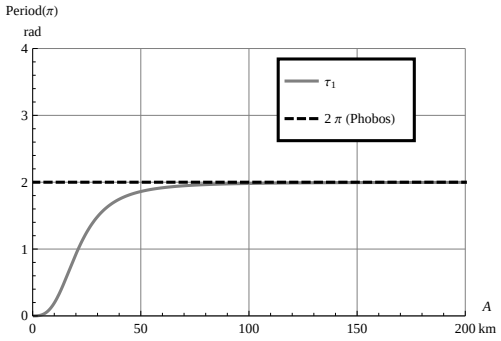

Fig. 5: Evolution of the revolution period τ_1 as a function of the epicycle's semi-minor axis A. The black dotted line represents the period of Phobos' orbit.

From Fig. 6 we notice that for increasing values of A both periods τ_2 and τ_3 are much higher than the reference period of the orbit of Phobos around Mars, which suggests that the drifting movement of the epicycles along the y direction tend to be slower for orbits with higher amplitudes.

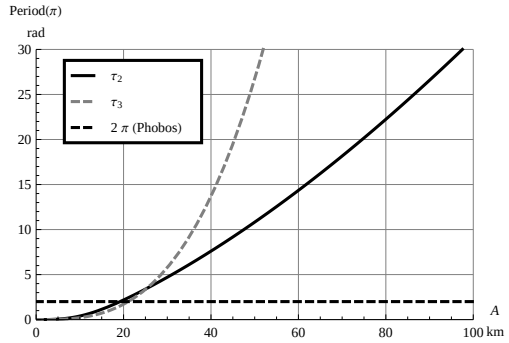

Fig. 6: Evolution of the periods τ_2 and τ_3 of the epicycle drift motion as a function of the epicycle's semi-minor axis A. The black dotted line represents the period of Phobos' orbit.

The remaining periodic motion is associated with the variations of the amplitude of the motion in the z direction which has frequency $2\omega_\beta$ and period:

$$\tau_4 = \frac{6\pi^2 A^3}{2\sqrt{2K^2 - EK - E^2}} \approx 6.47797A^3. \tag{20}$$

The period τ_4 behaves similarly to τ_3 meaning that for increasing values of the orbit's amplitude the period increases.

III. Approximating Phobos

Here we will describe the algorithm that was developed to approach Phobos: a sequential set of half epicycles. This algorithm will use the Differential Evolution method to minimize the algorithm cost function and compute the orbital parameters that provide the best cost value. After the nominal

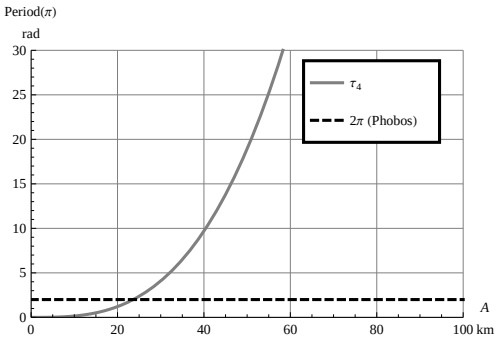

Fig. 7: Evolution of the period τ_4 associated to the z direction as a function of the epicycle's semi-minor axis A. The black dotted line represents the period of Phobos' orbit.

trajectory (analytical model) has been computed we will use the calculated orbital parameters to obtain the orbit's initial velocities and use them as initial conditions for the integration of the numerical model. In the end a comparison between the approximate analytical model and the numerical model is made along with some discussion of the results.

A. Approaching Strategy

The first step of developing an algorithm is the definition of its goal and the strategy to obtain it. In the present work we set the objective of establishing an algorithm for a controlled approach to Phobos from an initial orbit but we have yet to define the strategy to reach our goal.

Here we present the strategy to be adopted, which consists on using consecutively smaller epicycles to get closer to the Martian moon's surface. Departing from a point in the initial orbit (observation orbit) the S/C will perform a burn (ΔV) to reach a target point closer to Phobos in half epicycle. This process can then be repeated to approach the moon even further if desired. This strategy was chosen because it seemed fairly easy to execute and because it allows for some trajectory design freedom. This way it is possible to include interesting points on the approach trajectory to Phobos with the purpose of getting better video images of some point on the surface of the moon.

The problem of finding the orbit arch that connects two different points in space at a given time is a form of two boundary value problem (2PBVP). Such a problem can be solved by means of optimization by computing the system parameters that present the lowest cost function value associated with the boundary requirements. The optimization method to be used in the approach algorithm is called Differential Evolution (DE) method, which is a direct search method.

B. Inputs and Outputs

The inputs of the algorithm are the initial and final positions (km), the initial true anomaly (rad) and the number of control steps to be performed during the algorithm. Although we can choose the initial and final positions we limited them to coordinates on the $x-z$ plane and $y-z$ plane. This limitation was implied in part because in those planes it is much easier to compute an orbit transfer and using other points do not provide any advantage.

The initial true anomaly defines the position of Phobos relative to Mars at the start of the algorithm. Since the system is time dependent this means that for different initial true anomalies we will have different solutions because the position of Phobos in its orbit will be different and thus so it will be the influence of Mars on the trajectory.

The number of control steps basically defines the frequency at which the correction steps occur. The basic principle applied in this algorithm considers that each epicycle lasts half period to connect the initial position to the final position, nevertheless, as it was mentioned, the trajectory of the real dynamics tend to diverge from the epicycle computed with the analytic model and so correction steps are needed. The number of control steps is used to divide the half period into equally spaced step times and for each step time a correction is performed. The higher the number of control steps the smaller the step time, increasing the precision but also the computational effort as well as the energy (ΔV) consumed due to the higher number of corrections. A cost-benefit analysis can be made in order to decide which is the best number of control steps for each of the trajectories, if justified.

The outputs are basically the final positions and velocities of the non-corrected and corrected epicycles. These will be used as comparative parameters to assess the performance of the algorithm and the domain of validity of the developed model.

The required ΔV necessary to perform the corrections are also displayed in script while the algorithm is running and it is also an output that can be used to measure the cost-efficiency of the entire correction manoeuvre.

IV. Results

We now present and discuss the results obtained with the deduced solutions of the three dimensional ER3BP along with the test of the designed trajectory algorithm.

A. Model Validation

The comparison between model orbits and real orbits is important to assess the validity of the approximate analytical solutions obtained in section II-D. By comparing the differences between the two orbits for different parameters, we will be able to identify the regions for which the developed model can reproduce the real orbit behaviour described by the differential equations of the system (1).

To perform this assessment we will use five example orbits that are representative of the type of orbits that are likely to be used for an approximation trajectory to Phobos, and we consider the moon as being a spherical body with a radius of 13.5 [km].In Table I we present the set of parameters (dimensionless quantities) for the five orbits used to perform the comparisons. In Table I we can see that the orbit's amplitude varies from orbit to orbit, starting with a large amplitude (Set A) and progressively decreasing the amplitude for the following sets. This procedure will help us to understand how the amplitude

Set	A	δ_{x0}	δ_{y0}	γ_0	ϕ_0 [rad]	ψ_0 [rad]	f_0 [rad]
A	4.72013	-0.00290623	1.11807	0	-1.57019	6.28317	0
B	3.67306	-0.00626309	1.10211	0	-1.56912	-6.28319	0
C	3.15772	-0.0203936	2.1407	0	-1.56443	-0.402573	0
D	2.62624	-0.0172101	1.08574	0	-1.56434	6.28319	0
E	2.09465	0.00128818	0.0309118	0	4.71178	-6.28319	0
F	1.0527	0.00358671	0.00464257	0	4.70903	6.28319	0

TABLE I: Initial conditions for the set of sample orbits used in the coordinate evolution study.

affects the orbits behaviour and identify the differences when changing its value.

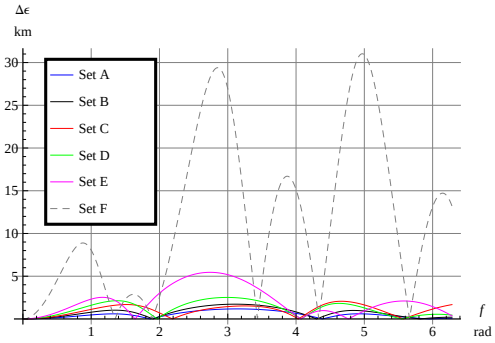

(a) Difference between model and real orbit over 2π for each set of parameters.

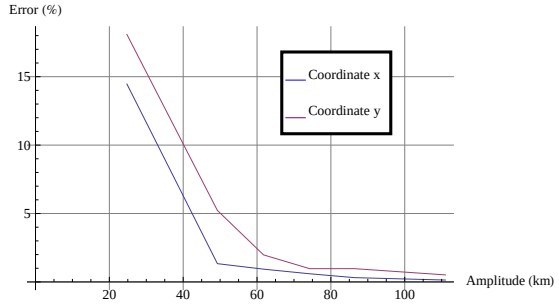

(b) Maximum relative error for the coordinates x and y

Fig. 8: Difference between model and real orbit over 2π for each set of parameters and Maximum relative error for the coordinates x and y

Figure 8a represents the evolution of the absolute difference (km) registered between model and real orbits for the different sets of parameters described in Table I. We see that the differences presented grow from Set A through Set F, which follows the inverse trend of the orbit's amplitude that decreases from Set A through Set F. This suggests that in fact the amplitude of the orbit affects the precision of the developed approximation when compared to the real dynamics of the system. It is clear that for large amplitudes both orbits behave similarly, but when the value of the orbit's amplitude decreases the differences start to grow. To support this conclusion it is also presented in Fig. 8b the maximum relative error for coordinate x and y registered for a period of 2π Here the error is directly related to the orbit's amplitude making it clear that for lower values of amplitude the difference between our model and the real dynamics start to increase significantly.

This result can be a consequence of the approximations made when we applied the method of variation of parameters to the obtained solutions as a way to account for Phobos' gravitational attraction as a perturbation. Due to its complicated form only first order terms were considered which might explain the appearance of differences in the coordinates evolution when the orbit's amplitude becomes smaller.

B. Approximation Trajectory Design

The next step will be the design of an approximation trajectory to Phobos using only, as initial and final positions, points laying on the $y-z$ plane or $x-z$ plane. This imposition will result in lower computational effort but it is also related to the fact that those are the two most interesting configurations to be studied, representing the cases when the orbit transfers occur at the extremities of the orbit.

These two strategies were named as a reference to the points were the actual orbit transfers occur. The $y-z$ plane transfers take as initial and final positions points in the $y-z$ plane or simply points that take 0 as x coordinate while the $x-z$ plane transfers take as initial and final positions points in the $x-z$ plane or, in other words, points that take zero as y coordinate.

To perform the study on how well the approximation strategies behave we will use the points in Table II and as initial true anomaly we will use the value 0. Fig. 9 shows a

Trajectory	Initial Pos. [km]	Interm. Pos. 1 [km]	Interm. Pos. 2 [km]	Interm. Pos. 3 [km]	Final Pos. [km]
YZ1	(0,150,0)	(0,-125,0)	(0,100,0)	(0,-75,0)	(0,50,0)
XZ1	(150,0,0)	(-125,0,0)	(100,0,0)	(-75,0,0)	(50,0,0)

TABLE II: Initial, intermediate and final positions for the trajectory design.

graphical representation of the resultant trajectories, where the dotted black lines represent the nominal trajectories computed by the trajectory algorithm, the gray lines represent the real spacecraft trajectories obtained by integration of (1) and the magenta lines represent the reference trajectory to be followed by the spacecraft at each orbit transfer. A quick inspection of the figures shows that the nominal trajectories pass on the stipulated way-points of Table II and that the real trajectories follow a similar behaviour by passing close to the required way-points, indicating that the behaviour of the real dynamics is emulated fairly well by the nominal designed trajectory. It is however worth mentioning that the closer we get to the moon, the bigger the differences between the nominal and real trajectories became, supporting the conclusions made in Section IV-A. Table III displays the specific energy necessary to perform the orbit transfers for the trajectories in Table II. The result is presented in specific energy (J/kg) because changes in the kinetic and potential specific energies of the vehicle are independent of the mass of the vehicle. Analysing

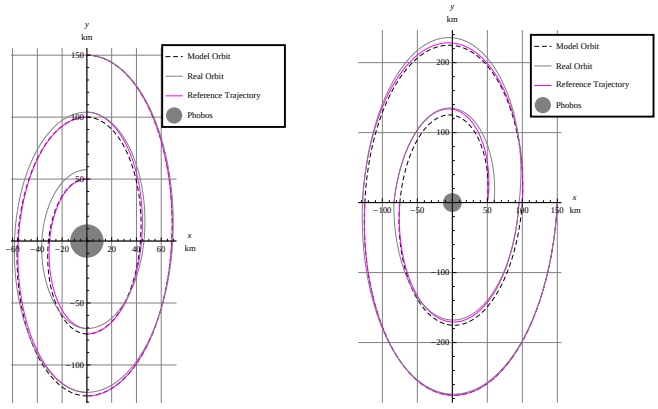

(a) Trajectory YZ1 (b) Trajecory XZ1

Fig. 9: Graphical representation of Trajectories YZ1-XZ1.

Table III we realise that the necessary specific energy is considerably higher for orbit transfers occurring in the $x-z$ plane, this result may be explained by the drift property that the orbit presents in the y-direction. If we consider that the orbit dynamics itself presents an oscillatory motion on the y-direction, than it is expected that performing an orbit transfer along such direction will be cheaper than performing it along a direction where there is no drift property. That is mainly because a small difference in the spacecraft velocity when standing along the y-direction will cause a drastic change in the trajectory whereas the same is not true when the spacecraft is positioned along the x-direction. The cost results evidence

Trajectory	Specific Energy [J/kg]
YZ1	8.98946
XZ1	27.4034

TABLE III: Specific energy spent on the trajectories YZ1-XZ2.

that the $y-z$ plane transfers strategy comes with a lower price, which is always a factor to be considered in the field of mission design. Thus, if no other factors are taken into account we believe that the best strategy to use is the $y-z$ plane transfer strategy, being the strategy used by default in the remaining of the present work.

C. 2D vs 3D

Until now we confined our analysis to planar cases $x-y$ (2D) but it is also important to get some insight on 3D cases and try to understand weather the introduction of the third coordinate produces significant differences in terms of orbit behaviour and energy consumption. For that purpose we will define a new 3D trajectories and will be using trajectory YZ1 a comparison term. The 3D trajectory, YZ3, is defined in Table IV and is simply the same as YZ1 but with a third coordinate different from 0.

Trajectory	Initial Pos. [km]	Interm. Pos. 1 [km]	Interm. Pos. 2 [km]	Interm. Pos. 3 [km]	Final Pos. [km]
YZ3	(0,150,10)	(0,-125,-10)	(0,100,10)	(0,-75,-10)	(0,50,10)

TABLE IV: Initial, intermediate and final positions for the 3D trajectory design.

Trajectory	Specific Energy [J/kg]	Note
YZ3	12.3252	+ 37% than YZ1

TABLE V: Specific energy spent on the trajectories YZ3.

The results of the 3D trajectory design are presented in Fig. 10 suggesting that the introduction of the third coordinate does not change the planar orbit behaviour, which is expected since the oscillations in the z direction are much slower than Phobo's orbital period as proven in section II-E. This can be verified by simply comparing Fig. 10a with the graphical representations of YZ1 in Fig. 9, which shows that the shape of the 2D projections of the trajectories are identical. Regarding the

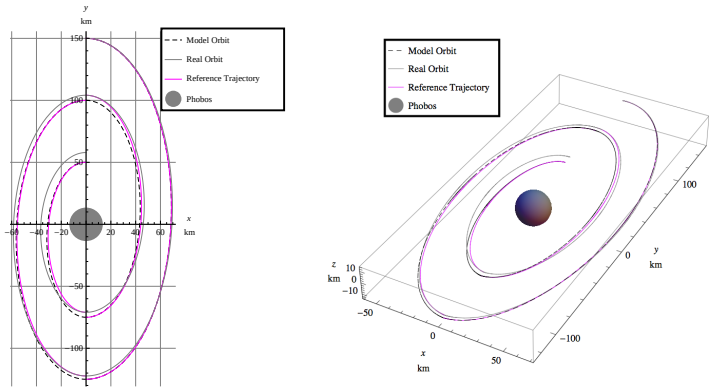

(a) 2D (b) 3D

Fig. 10: Graphical representation of Trajectory YZ3.

specific energy consumption the results show that in fact there is an increase of energy consumption when comparing with the values registered in the planar trajectory. This increment of 33% is not strange since in the 3D cases there is one more coordinate to control.

D. Controlled Trajectories

In order to compensate for the first order approximation of part of Phobos' gravitational attraction we introduced a control strategy capable of computing the necessary corrections (ΔV) to be applied to the real trajectory so that it follows the reference trajectory given by our model. We will apply the control strategy to the example YZ1 and evaluate the resultant improvements as well as the cost associated with the corrections performed. As a result the given inputs for the algorithm are the set of positions in table II, the initial true

anomaly is zero and the number of control steps is 25. The initial true anomaly value is zero to be in line with what was used in the computation of YZ1. The number of control steps to be performed throughout the control algorithm was chosen to be 25 so that a balance is kept between computational time and algorithm performance.

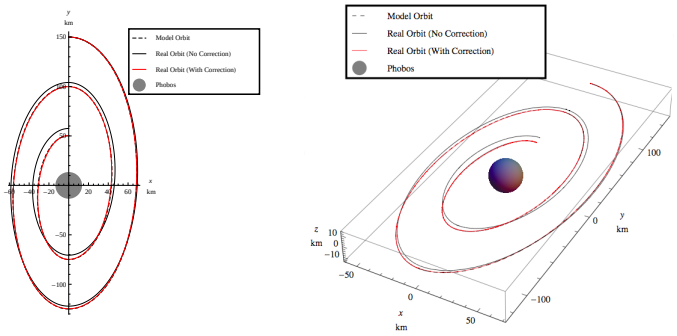

(a) 2D

(b) 3D

Fig. 11: Graphical representation of Trajectory YZ1 using the control strategy.

The results obtained with the controlled algorithm (Fig. 11) show that there is a clear improvement of the real orbit behaviour as expected, which now follows more accurately the reference (Model Orbit). This is an important outcome for the purpose of trajectory design because it allows us to compensate for the rough approximation of the gravitational potential made to obtain the analytical solution of the three dimensional ER3BP, and guarantee that the real orbit follows the predefined trajectory computed with the developed solution.

The analysis of the energy consumption resulting from the introduction of control steps returned some interesting results. Comparing the energy values required to perform the necessary orbit transfers (Tables III and VI) we realise that the application of the control strategy resulted in lower values of energy consumption to perform the transfers. This outcome may be a consequence of the improvement made on the trajectory behaviour, suggesting that for the case where no control strategy is applied the orbit transfer ΔV is higher in order to compensate for the divergences verified between the real orbit and the reference model orbit (Fig. 9). On the other hand, for the controlled case we are applying timely corrections to guarantee that the real orbit is correctly tracking the reference model orbit, which also requires consumption of energy (Table VI). The total energy consumption is, as expected, larger when controlled is used, however, it's higher value is still within the same order of magnitude as the value obtained when no controlled is applied, which indicates that the control strategy is affordable from the point of view of energy consumption. Figure 12 represents the evolution of the magnitude of the impulsive shots ($\Delta V's$) for each control step showing that throughout the correction process the magnitude of the impulses tends to increase. This means that the closer

Trajectory	Orbit Transfer Energy [J/kg]	Control Energy [J/kg]	Total Energy [J/kg]
YZ1 (Correction)	5.661799	5.3744	11.036199

TABLE VI: Specific energy spent on the trajectories YZ1-YZ2 when control is applied.

the S/C gets to Phobos the higher is the effort necessary to perform the trajectory corrections, which is in line with the theory that the real orbit dynamics differs from the developed model dynamics when we get closer to Phobos.

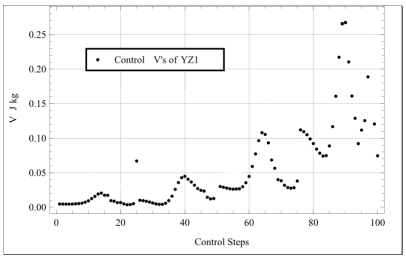

Fig. 12: ΔV evolution at each control step.

E. Landing on Phobos

We considered the possibility of deorbiting from a QSO directly to the surface of Phobos because we felt that it would be an interesting case that is worth examining. With the purpose of assessing the feasibility of such approach we decided to test three different examples. For all the examples we selected $(0, 50, 0)$ [km] as the initial point and $(13.5, 0, 0)$ [km] , $(9.55, 9.55, 0)$ [km] and $(6.75, 6.75, 9.55)$ as landing points for examples 1, 2 and 3 respectively. The results (Fig. 13) are consistent and show that in fact it is possible to design a deorbit path capable of delivering the spacecraft directly from a QSO to the surface of the moon. It is visible that the corrected real orbit tracks the reference model orbit quite well in all the cases, which proves that the designed algorithm allows the selection of the desired landing position. The major concern about this strategy is related to the braking phase, which has not been studied in the present work. The S/C final velocity components are $(V_x, V_y, V_z) = (-3.63035, -11.2872, -3.11375 \times 10^{-8})$ [m/s] for the first example, $(V_x, V_y, V_z) = (-3.48257, -10.8702, -1.44923 \times 10^{-6})$ [m/s] for the second and $(V_x, V_y, V_z) = (-4.99951, -7.64315, -1.94945)$ [m/s] for the last example, but we believe they can be easily compensated using small braking burns in the last moments of the landing phase. In terms of energy costs all the examples show a similar behaviour (Fig. 14), starting with small $\Delta V's$ at the beginning of the manoeuvre but with an increasing trend towards the end of the path.

Further analysis should be made in order to evaluate which approach is the more suitable, however, with the results gatherer throughout our inspection and given the results obtained we believe it is viable the use of the developed algorithm as tool for trajectory design in the vicinity of the Martian moon Phobos.

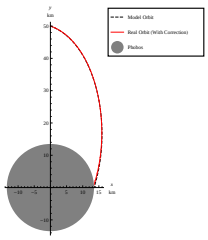

(a) Example 1

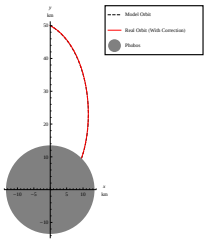

(b) Example 2

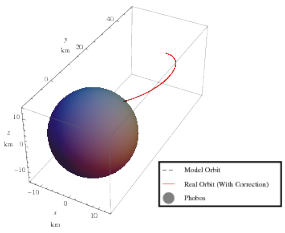

(c) Example 3

Fig. 13: Landing Approach.

V. Conclusions

The present work considered the development and implementation of an algorithm capable of computing an approximation trajectory to approach the Martian moon Phobos. After having modelled the S/C dynamics near the moon, where only the influence of Mars' and Phobo's gravitational potential was taken into consideration, the associated analytical system of equations describing the problem was presented and an approximate analytical solution was obtained for the case of small gravitational parameter μ and eccentricity of the smaller primary orbit e.

A strategy to approach Phobos from an observation QSO was designed using a Differential Evolution search method to solve the two point boundary value problem of obtaining suitable solutions given the desired initial and final positions of the desired trajectory. A comparison between model and real orbits was used as validation method for the obtained analytical solution of the problem, which enabled the understanding of the limitations of the analytical approximation.

A control strategy was designed as a method to extend the validity of the developed model to the vicinity of Phobos, region where the simple model has shown some flaws. Simulations of approximation trajectories were finished with success, which included an energy cost analysis proving the feasibility of such solutions in terms of dynamical behaviour but also in terms of power needs.

In future work it would be challenging the use of a second-order approximation to the gravitational potential of Phobos, which could extend the validity of the attained solution to regions closer to the moon's surface providing a more accurate solution for mission design purposes. Also, the J2 of Phobos is large and should be included, as it will influence the orbit considerably.

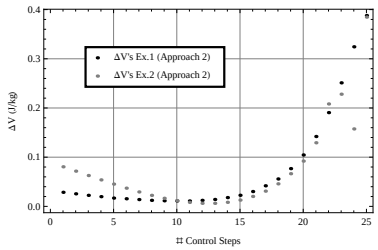

(a) ΔV evolution at each control step for Ex. 1 and 2.

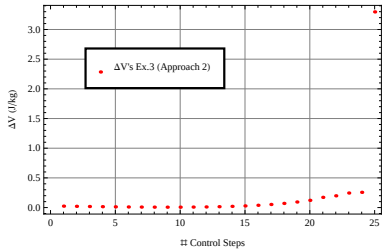

(b) ΔV evolution at each control step for Example 3.

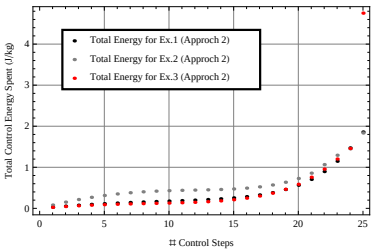

(c) Total energy evolution.

Fig. 14: Energy cost for landing manoeuvre.

References

[1] P. J. S. Gil and J. Schwartz, "Simulations of Quasi-Satellite Orbits Around Phobos," *Journal of Guidance, Control, and Dynamics*, vol. 33, no. 3, 2010.

[2] S. R. K. K. Mukhin, L. M. and A. Zakharov, "Phobos, deimos mission," *Concepts and Approaches for Mars Exploration*, pp. 230–232, July 2000.

[3] V. G. Szebehely, *Theory of Orbits, The Restricted Problem of Three Bodies*. Academic Press, 1967.

[4] A. Y. Kogan, "Distant Satellite Orbits in the Restricted circular problem of Three Bodies," *Cosmic Research*, vol. 26, no. 6, pp. 813–818, 1989.

[5] D. Benest, "Libration Effects for Retrograde Satellites in the Restricted Three-Body Problem," *Celestial Mechanics*, vol. 13, no. 2, pp. 213–215, 1976.

[6] W. Boyce and R. DiPrima, *Elementary Differential Equations and Boundary Value Problems*. John Wiley & Son, Inc., 2005.

[7] D. Zwillinger, *Handbook of Differential Equations*. Academic Press, 1997.

[8] M. Efroimsky, "Equations for the keplerian elements: Hidden symmetry," 2002, preprint # 1844 of the IMA.